Viscous Torque and Dissipation in the Inner Regions of a Thin Accretion Disk: Implications for Measuring Black Hole Spin

The Astrophysical Journal, 676:549–561, 2008 March 20

VISCOUS TORQUE AND DISSIPATION IN THE INNER REGIONS OF A THIN ACCRETION DISK: IMPLICATIONS FOR MEASURING BLACK HOLE SPIN

Rebecca Shafee,[1] Ramesh Narayan,[2] and Jeffrey E. McClintock[2]
Received 2007 May 16; accepted 2007 November 12

ABSTRACT

We consider a simple Newtonian model of a steady accretion disk around a black hole. The model is based on height-integrated hydrodynamic equations, α-viscosity, and a pseudo-Newtonian potential which results in an innermost stable circular orbit (ISCO) that closely approximates the one predicted by general relativity. We find that, as the disk thickness H/R or the value of α increases, the hydrodynamic model exhibits increasing deviations from the standard thin disk model of Shakura and Sunyaev. The latter is an analytical model in which the viscous torque is assumed to vanish at the ISCO. We consider the implications of the results for attempts to estimate black hole spin by using the standard disk model to fit continuum spectra of black hole accretion disks. We find that the error in the spin estimate is quite modest so long as $H/R \leq 0.1$ and $\alpha \leq 0.2$. At worst, the error in the estimated value of the spin parameter is 0.1 for a nonspinning black hole; the error is much less for a rapidly spinning hole. We also consider the density and disk thickness contrast between the gas in the disk and that inside the ISCO. The contrast needs to be large if black hole spin is to be successfully estimated by fitting the relativistically broadened X-ray line profile of fluorescent iron emission from reflection off an accretion disk. In our hydrodynamic models, the contrast in density and thickness is low when $H/R \gtrsim 0.1$, suggesting that the iron line technique may be most reliable in extremely thin disks. We caution that these results have been obtained with a viscous hydrodynamic model. While our results are likely to be qualitatively correct, quantitative estimates of, e.g., the magnitude of the error in the spin estimate, need to be confirmed with MHD simulations of radiatively cooled thin disks.

Subject headings: accretion, accretion disks — binaries: close — black hole physics — X-rays: stars

1. INTRODUCTION

Recently, we reported spin estimates of three black holes (BHs) in Galactic X-ray binaries (Shafee et al. 2006; McClintock et al. 2006, hereafter S06 and M06, respectively). The results were obtained by fitting the soft X-ray continuum spectra of these systems in the thermal state (Remillard & McClintock 2006) to a general relativistic, multicolor blackbody, thin disk model (KERRBB; Li et al. 2005), which includes the effect of spectral hardening (Davis et al. 2005). In this method, which was pioneered by Zhang et al. (1997), we assume a razor-thin disk that terminates at the innermost stable circular orbit (ISCO). In addition, we assume that the viscous torque vanishes at the ISCO and that there is no energy dissipation or angular momentum loss inside the ISCO. These are standard assumptions in the theory of accretion disks (e.g., Shakura & Sunyaev 1973; Frank et al. 2002) and correspond to what we refer to in this paper as the "standard disk model." However, there has been debate in recent times as to the validity of the assumptions.

The stress responsible for angular momentum transport in a thin accretion disk is likely to be magnetic (Balbus & Hawley 1991). If this is the case, an argument could be made for a nonzero stress at the ISCO, coupled with considerable dissipation near and inside the ISCO (Krolik 1999; Gammie 1999). These effects could cause important deviations from the standard disk model (Krolik & Hawley 2002), perhaps invalidating our spin determinations.

Afshordi & Paczyński (2003), following earlier work by Abramowicz & Kato (1989) and Paczyński (2000), suggested that the torque at the ISCO increases with increasing disk thickness. Motivated by their work, we argued in M06 that deviations from the standard disk model are likely to be serious only for thick disks. We thus restricted our attention to relatively thin disks with height-to-radius ratios of $H/R < 0.1$. The present paper is an attempt to verify whether or not such thin disks do indeed behave like the standard disk model.

In addition to the debate over the validity of using the standard disk theory to model the continuum spectra of realistic disks, another relevant issue in attempting to estimate BH spin is the relative merit of the continuum fitting method compared to fitting the relativistically broadened fluorescent iron line in the X-ray spectrum. Both methods have been proposed as a means of estimating BH spins, and it is of interest to understand how well the assumptions of each are satisfied by real disks. The models currently used by the iron line method assume that the line emissivity peaks at the ISCO, drops abruptly to zero inside the ISCO, and decreases steeply as a broken power law outside the ISCO (e.g., Brenneman & Reynolds 2006, hereafter BR06). This requires, among other things, a significant drop in matter density (Fabian 2007) or disk thickness (Nayakshin et al. 2000; Nayakshin & Kazanas 2002) inside the ISCO. A second motivation for the present paper is therefore to check the validity of the assumed line emissivity profile.

Our analysis is based on a nonrelativistic hydrodynamic model of an accretion disk. We present global numerical solutions of the differential equations governing the fluid flow, assuming that the accretion disk is steady, axisymmetric and in hydrostatic equilibrium in the vertical direction, and using a pseudo-Newtonian model for the gravitational potential. We do not include magnetic fields explicitly, but assume an effective viscosity described by the α prescription (Shakura & Sunyaev 1973). We also assume an adiabatic index $\gamma = 1.5$, which corresponds to approximate equipartition between gas and magnetic pressure (Quataert & Narayan 1999).

[1] Harvard University, Department of Physics, 17 Oxford Street, Cambridge, MA 02138.
[2] Harvard-Smithsonian Center for Astrophysics, 60 Garden Street, Cambridge, MA 02138.

Our primary interest is in accretion disks in the rigorously defined thermal state (see Table 2 in Remillard & McClintock 2006) with $H/R < 0.1$, as these are the systems of most interest for our work on BH spin (M06). Since the value of the viscosity parameter α for such disks is a matter of debate, we try different constant values, $\alpha = 0.01, 0.1$, and 0.2. We also consider a variable-α prescription (eq. [22]) inspired by the MHD simulations of Hawley & Krolik (2002, hereafter HK02). For nonspinning BHs, we use the pseudo-Newtonian potential of Paczyński & Wiita (1980, hereafter PW80), and for spinning black holes we use the pseudo-Kerr model of Mukhopadhyay (2002). The numerical framework for our calculations is similar to that used by Narayan et al. (1997), viz., we use a relaxation method to solve the equations from the sonic radius R_s to the outer edge of the disk ($\sim 10^5 R_s$), and we then integrate inward from R_s to the event horizon.

The paper is organized as follows. We discuss in § 2 the theory and computational method. We then discuss in § 3 our numerical disk solutions, focusing on the magnitude of the stress at the ISCO, the amount of viscous dissipation near and inside the ISCO, and the density and disk thickness contrast across the ISCO. We then compute in § 4 the emitted spectra of our numerical disks for different values of H/R and α and investigate the error we make when we estimate the spin of a BH via the continuum fitting method assuming the standard disk model. We conclude in § 5 with a discussion.

2. THE MODEL

2.1. *Gravity*

In order to focus our attention on the key physics of the problem and to avoid being distracted by technical details, we consider a simple viscous hydrodynamic accretion disk in a Newtonian gravitational potential. Since the presence of an ISCO is essential for our analysis, we simulate relativistic gravity in this Newtonian model by means of a modified gravitational potential. For a nonspinning BH, we make use of the PW80 potential,

$$\Phi = -\frac{GM}{R - 2R_g}, \tag{1}$$

where M is the BH mass, G is the gravitational constant, and $R_g = GM/c^2$. The Keplerian angular velocity $\Omega_{\rm K}$ at a radius R from the BH is

$$\Omega_{\rm K} = \frac{(GM)^{1/2}}{(R - 2R_g)R^{1/2}}. \tag{2}$$

In the case of a spinning BH we use the pseudo-Kerr model of Mukhopadhyay (2002) in which the gravitational acceleration of a test particle in a Keplerian orbit at a distance R from the BH is

$$F = -\nabla\Phi = \frac{c^4}{GM}\frac{(r^2 - 2a_*\sqrt{r} + a_*^2)^2}{r^3[\sqrt{r}(r-2) + a_*]^2}, \tag{3}$$

where $r = R/R_g$, $a_* = a/M = J/(GM^2/c)$ is the dimensionless spin of the BH, and $-1 < a_* < 1$. The Keplerian angular velocity at radius R is then

$$\Omega_{\rm K} = \frac{c^3}{GM}\frac{(r^2 - 2a_*\sqrt{r} + a_*^2)}{r^2[\sqrt{r}(r-2) + a_*]}. \tag{4}$$

2.2. *Hydrodynamics*

We assume a steady axisymmetric disk in hydrostatic equilibrium in the vertical direction. In the equations that follow, which have a long history in accretion disk theory (e.g., Paczyński & Bisnovatyi-Kogan 1981; Muchotrzeb & Paczyński 1982; Kato et al. 1988; Abramowicz et al. 1988; Popham & Narayan 1991; Narayan & Popham 1993; Chen & Taam 1993; Narayan et al. 1997; Chen et al. 1997), we denote density, sound speed, radial velocity, angular velocity, Keplerian angular velocity, and vertical half-thickness by ρ, c_s, v_R, Ω, $\Omega_{\rm K}$, and H, respectively. All these parameters are taken to be functions of the cylindrical radius R only. Because of the assumption of steady state, the Lagrangian time derivative $D/Dt = \partial/\partial t + \boldsymbol{v}\cdot\nabla$ becomes $D/Dt = v_R\, d/dR$. After vertical and then radial integration, the continuity equation takes the form

$$4\pi\rho v_R R H = -\dot{M} = \text{const}, \tag{5}$$

where $H = c_s/\Omega_{\rm K}$. The momentum equation is

$$\rho(\boldsymbol{v}\cdot\nabla)\boldsymbol{v} = -\nabla P - \rho\nabla\Phi + \rho\Omega^2\boldsymbol{R} + \rho\nabla\cdot\boldsymbol{\sigma}, \tag{6}$$

where $\boldsymbol{\sigma}$ is the stress tensor. We assume that the only nonzero component of $\boldsymbol{\sigma}$ is $\sigma_{R\Phi} = -\alpha P$ (α prescription; Shakura & Sunyaev 1973), where P is the total pressure and we write $P = \rho c_s{}^2$. The radial component of the momentum equation gives

$$v_R\frac{dv_R}{dR} = -(\Omega_{\rm K}^2 - \Omega^2)R - \frac{1}{\rho}\frac{d}{dR}(\rho c_s^2), \tag{7}$$

and conservation of angular momentum gives

$$\frac{\rho v_R}{R}\frac{d}{dR}(\Omega R^2) = \frac{1}{R^2 H}\frac{d(R^2 H\sigma_{R\Phi})}{dR}. \tag{8}$$

The latter equation can be integrated to obtain

$$\Omega R^2 - j = -\frac{\alpha c_s^2 R}{v_R}, \tag{9}$$

where ΩR^2 is the specific angular momentum of the gas at radius R and j is an integration constant. We can interpret j as the specific angular momentum of the accreting gas at the radius where the stress goes to zero.

Lastly, we write the energy conservation equation in terms of the Lagrangian derivative of the specific entropy,

$$\rho T\frac{Ds}{Dt} = q^+ - q^- = fq^+, \tag{10}$$

where s is the specific entropy per unit mass, and q^+ and q^- are the volume rate of heating and cooling of the gas, respectively. Following Narayan et al. (1997) we take the cooling rate to be a factor $(1 - f)$ of the heating rate. Narayan et al. used $f = 1$ because they were modeling advection-dominated accretion flows. Since we are interested primarily in thin disks, we use small values of f, i.e., substantial cooling, and we tune the value of f to achieve the desired disk thickness (eq. [19]). The heating of the gas is due to viscous dissipation, which gives $q^+ = \nu\sigma R\, d\Omega/dR$. Using the relationship $\epsilon = P/(\gamma - 1)$, where ϵ is the thermal energy per unit volume and γ is the adiabatic index (we use $\gamma = 1.5$), we can write

$$\rho T\frac{Ds}{Dt} = \frac{\rho v_R}{\gamma - 1}\frac{dc_s^2}{dt} - c_s^2 v_R\frac{d\rho}{dR}. \tag{11}$$

Thus, the energy equation takes the form

$$\frac{\rho v_R}{\gamma-1}\frac{dc_s^2}{dR}-c_s^2 v_R\frac{d\rho}{dR}=-f\alpha\rho c_s^2 R\frac{d\Omega}{dR}. \tag{12}$$

2.3. *Boundary Conditions and Numerical Method*

We use a relaxation method to obtain numerical solutions of the above differential equations. In the computations, we define $x = R/R_s$ as the spatial variable and covered the region $x = 1$ to 10^5 using 1000 grid points. The grid has a nonuniform spacing, with more grid points near the inner boundary $x = 1$. In solving the equations, we set $-4\pi\rho v_R RH = \dot{M} = 1$, and in order to simplify the equations we substitute for ρ using equation (5). Thus, we are left with three unknown functions of R: $v_R(R)$, $c_s^2(R)$, and $\Omega(R)$. In addition, we have two unknown constants, j and R_s, which we treat as eigenvalues. To solve for these quantities, we use equations (7), (9), and (12), supplemented with five boundary conditions.

Narayan et al. (1997) showed that solutions of the disk model described in § 2.2 tend to be nearly self-similar over a wide range of radius. Assuming self-similarity (following Narayan & Yi 1994), we can obtain the following analytic solution of the equations (the subscript "ss" refers to self-similar),

$$c_{s,\mathrm{ss}}^2(R)=c_0^2\frac{GM}{R},\quad c_0^2=\frac{2}{5+2\epsilon'+\alpha^2/\epsilon'},\quad \epsilon'=\frac{5/3-\gamma}{f(\gamma-1)}, \tag{13}$$

$$v_{R,\mathrm{ss}}(R)=v_0\sqrt{\frac{GM}{R}},\quad v_0=-\alpha\sqrt{\frac{c_0^2}{\epsilon'}}, \tag{14}$$

$$\Omega_{\mathrm{ss}}(R)=\Omega_0\Omega_{\mathrm{K}},\quad \Omega_0=\sqrt{\frac{2\epsilon'}{5+2\epsilon'+\alpha^2/\epsilon'}}. \tag{15}$$

We use this self-similar solution to set boundary conditions at the outer boundary R_{out},

$$v_R(R_{\mathrm{out}})=v_0\sqrt{\frac{GM}{R_{\mathrm{out}}}}, \tag{16}$$

$$c_s^2(R_{\mathrm{out}})=c_0^2\frac{GM}{R_{\mathrm{out}}}, \tag{17}$$

$$\Omega(R_{\mathrm{out}})=\Omega_0\Omega_{\mathrm{K}}. \tag{18}$$

From the above relations it can be shown that, at the outer boundary, the vertical scale height H satisfies

$$\frac{H}{R}=\sqrt{\frac{2}{5+2\epsilon'+\alpha^2/\epsilon'}}. \tag{19}$$

Therefore, for a given value of γ, we can vary the disk thickness H/R by changing f. For $\gamma = 1.5$, $f = 0.000035$ and 0.0035 give $H/R = 0.01$ and 0.1, respectively. Once set at the outer edge, the value of H/R remains constant over most of the disk, becoming smaller only near and inside the ISCO. Note that, for the thin disk models that we consider in this paper which have $H/R \leq 0.1$, the advection parameter f is very much less than unity. This means that radiative cooling (which is $\propto 1-f$) dominates by a huge factor over energy advection ($\propto f$). We briefly discuss thicker advection-dominated solutions in § 5.

The inner boundary is at the sonic radius, $R = R_s$, which is a singular point of the differential equations. Following standard methods, we obtain the following regularity conditions at R_s,

$$v_R^2-\frac{2\gamma}{\gamma+1}c_s^2=0, \tag{20}$$

$$\left(\Omega_{\mathrm{K}}^2-\Omega^2\right)R-c_s^2\frac{2\gamma}{\gamma+1}\left(\frac{1}{R}-\frac{d\ln\Omega_{\mathrm{K}}}{dR}\right)-c_s^2\frac{\gamma-1}{\gamma+1}\frac{f\alpha R}{v_R}\frac{d\Omega}{dR}=0. \tag{21}$$

Equations (16)–(18) and (20)–(21) provide the five boundary conditions we need to find a unique solution. Once we have obtained the solution between $R = R_s$ and $R = R_{\mathrm{out}}$ via the relaxation method, we use the solution at $R = R_s$ as initial conditions and integrate the equations from R_s down close to the BH event horizon.

We should emphasize that we do not set any boundary condition at the ISCO. Instead, we apply the boundary conditions at the sonic radius, whose position is computed self-consistently for each solution. Further, even at the sonic radius, the viscous torque is not set to zero—the torque is computed self-consistently and is allowed to continue smoothly inside the ISCO. The numerical solutions we obtain are thus superior to the standard disk model and can be used to check the validity of the latter. In particular, we can estimate what error one makes in the standard disk model as a result of the zero-torque boundary condition.

3. RESULTS

3.1. *Numerical Solutions*

Figure 1 shows model results for a nonspinning BH. We consider two disk thicknesses, $H/R = 0.01$ (*solid lines*) and 0.1 (*dotted lines*). In all four panels the vertical line shows the position of the ISCO ($R = 6R_g$). We use $G = M = c = 1$, so that the unit of velocity and time are c and GM/c^3, respectively, and set $\dot{M} = 1$. Most of our models correspond to a constant value of α. However, we also consider a model in which α varies as a function of R,

$$\alpha=\frac{16.8}{(R/R_g)^3}+0.1, \tag{22}$$

which closely reproduces the effective profile of α found by HK02 (see their Fig. 4). We refer to this as the "variable-α model."

Figure 1*a* shows the variation of the sound speed squared c_s^2 as a function of radius R. For a given thickness, the different α models overlap at large radii and are only distinguishable in the inner region of the disk. Here and in the figures that follow, the magenta, blue, red, and green lines refer to the $\alpha = 0.01$, 0.1, 0.2, and variable-α models, respectively. Figure 1*b* shows the radial infall velocity v_R of the accreting gas. We see that, between the ISCO and the event horizon, v_R increases rapidly regardless of the value of α. The variable-α model almost completely overlaps with the $\alpha = 0.1$ model even at large radii. Figure 1*c* shows the angular velocity Ω and Keplerian angular velocity Ω_{K}. The profiles of Ω for the different values of α and H/R are not distinct and are represented by the single dotted line. The solid red line corresponds to the Keplerian angular velocity. Note that the gas orbits in a nearly Keplerian fashion until it reaches the ISCO. Thereafter, the hydrodynamic forces maintain an orbital motion that becomes increasingly sub-Keplerian as the gas approaches the event horizon. Figure 1*d* shows the gas density ρ as a function of radius. As in the case of the sound speed (Fig. 1*a*), the density reaches a maximum outside the ISCO and then decreases rapidly near the

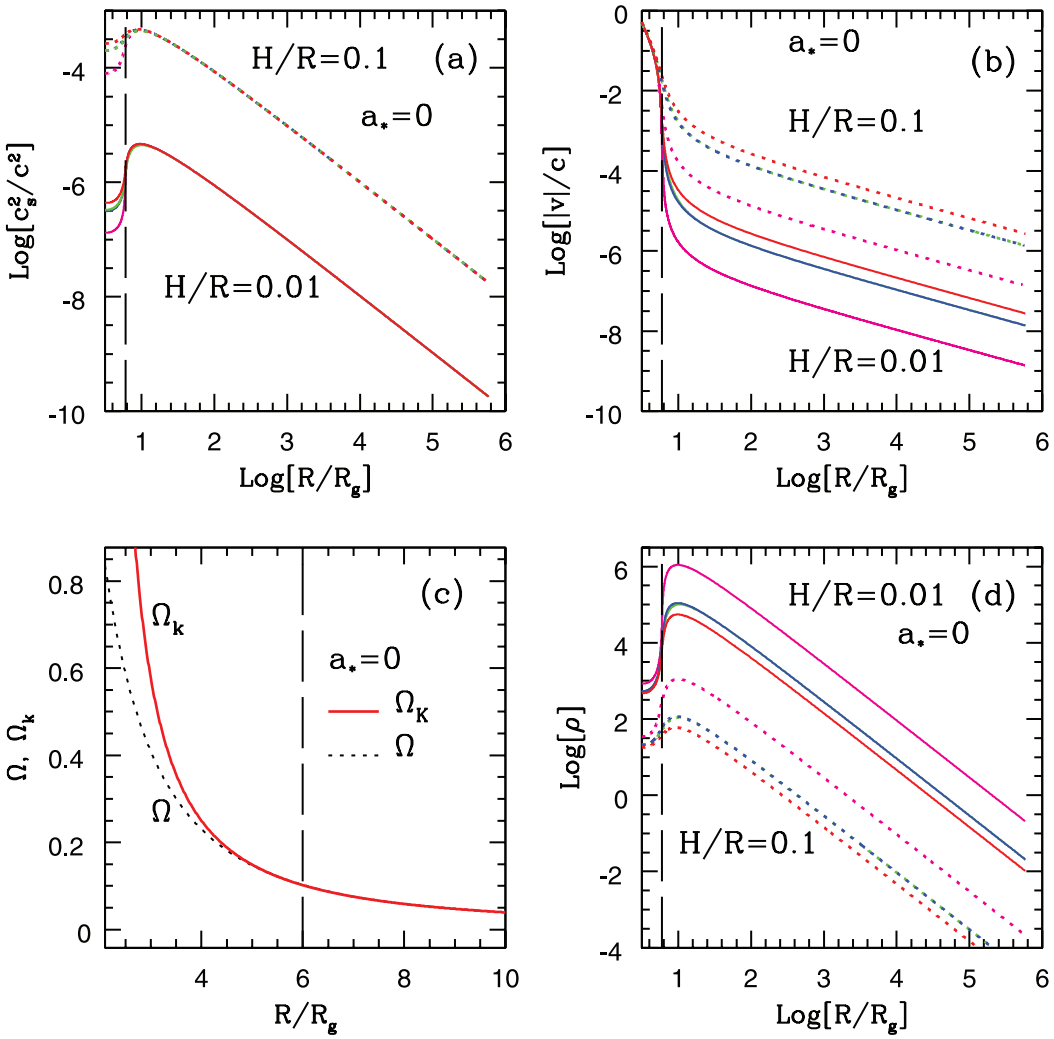

FIG. 1.—Disk parameters for a nonspinning BH: (*a*) sound speed, (*b*) radial velocity, (*c*) angular velocity, and (*d*) density. In (*a*), (*b*), and (*d*), the solid and dotted lines correspond to $H/R = 0.01$ and 0.1, respectively; where distinct, the magenta, blue, red, and green lines represent $\alpha = 0.01$, 0.1, and 0.2, and variable α (eq. [22]), respectively. In all three panels, the variable-α model is nearly coincident with the $\alpha = 0.1$ model. In (*c*), the Keplerian velocity is plotted as a solid red line. Because the angular velocity profile of the four models are nearly identical, we represent them by a single dotted line. The radius of the ISCO, $R = 6R_g$, is indicated in all four panels by the vertical dashed line. All numerical values correspond to $G = c = M = 1$, $\dot{M} = 1$. In (*c*), the unit of angular velocity is $(GM/c^3)^{-1}$. In (*d*), the unit of ρ is $c^6/(G^3M^2)$.

event horizon. In this plot, too, the variable-α model coincides with the $\alpha = 0.1$ model.

Figure 2 is in the same format as Figure 1 and presents our results for a spinning BH with $a_* = 0.95$. The principal difference from the previous figure is that the ISCO (*vertical dashed line*) is now located at $R = 1.937R_g$. We consider the same values of α and H/R as in Figure 1, but there is no variable-α model in this case because HK02 considered only a nonspinning BH.

3.2. *Matter Density, Disk Thickness, and the Iron Line Method*

Before presenting our main results in the following subsections, we briefly consider the implications of our models for the determination of spin via the iron line method. The source geometry and illumination law for producing the fluorescence iron line are probably the largest uncertainties in the line fitting method (Reynolds & Begelman 1997). If we assume the steepest law that is suggested by Reynolds & Begelman (1997), then the irradiating flux $F_X \sim R^{-3}$. Let us write the emissivity function in the form $f_{Fe}F_X$, where f_{Fe} is an efficiency factor. In this section we investigate if the existing models of f_{Fe} in the literature agree with our hydrostatic models.

The currently favored iron line models (BR06) assume that the iron line emission is restricted between R_{ISCO} and an outer radius R_{out} and that, within this region, the line profile is fitted by a broken power law. BR06 find that the emissivity varies as $\sim R^{-6}$ between the break radius R_{br} and R_{ISCO}, and as $\sim R^{-3}$ between R_{br} and R_{out}. For $F_X \sim R^{-3}$, this implies the following form for the efficiency function,

$$f_{Fe(BR06)} = \begin{cases} 0, & R < R_{ISCO}, \\ 1/R^3, & R_{ISCO} \le R \le 3R_{ISCO}, \\ \text{const}, & 3R_{ISCO} < R. \end{cases} \quad (23)$$

Below we discuss the two main theories regarding the physical parameters that might affect the emissivity profile.

Constant-density models (Ross & Fabian 1993; Życki et al. 1994; Ross et al. 1999) predict that the line emissivity is dependent on the ionization parameter, which is proportional to F_X/ρ, where ρ is the gas density and F_X is the illuminating flux. It is argued that the gas density drops to very low values inside the ISCO. As a result, the region inside the ISCO has a very high ionization parameter, which in turn produces negligible iron line

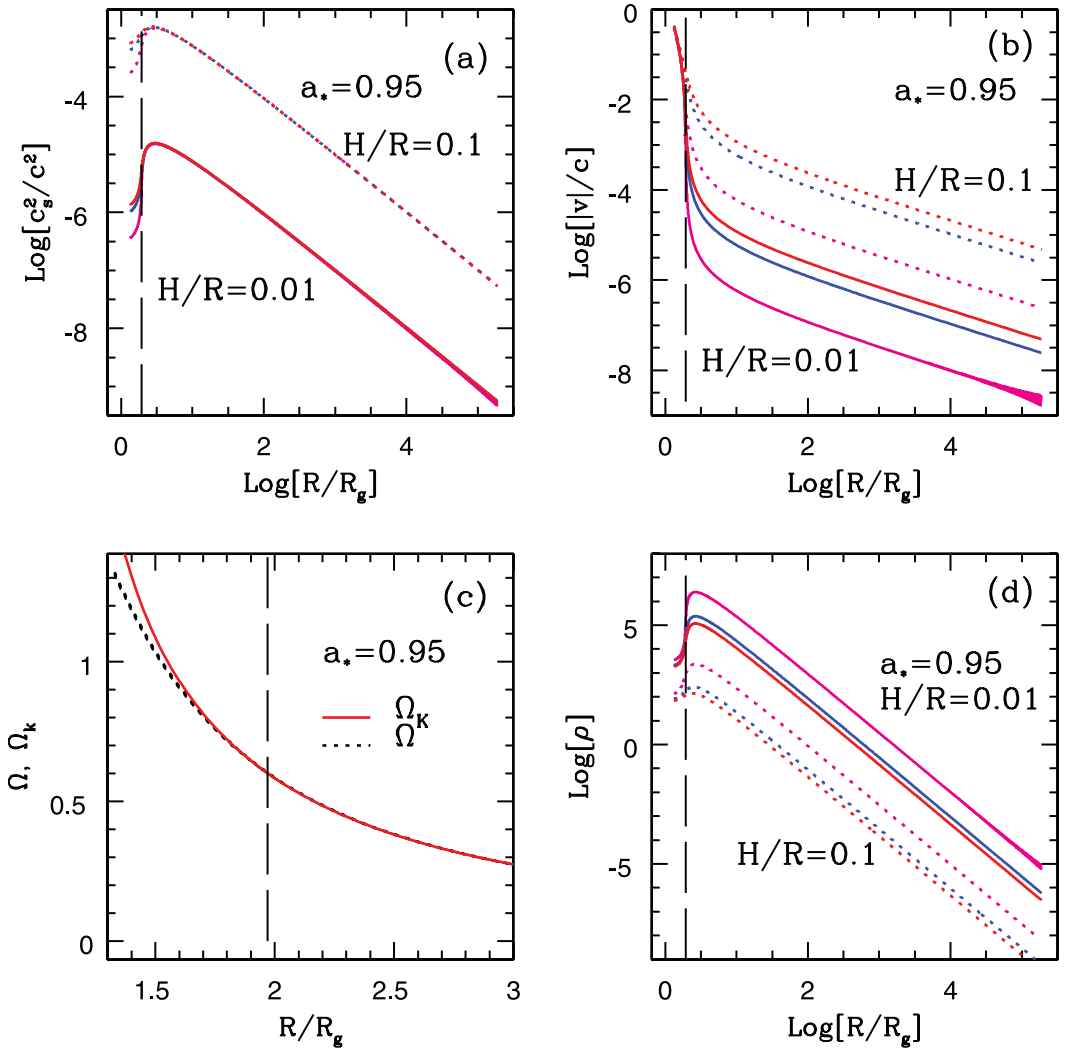

FIG. 2.—Same as Fig. 1, but for a spinning BH with $a_* = 0.95$. The vertical dashed line shows the ISCO at $R = 1.937R_g$. There is no variable-α model in this case (see text), and hence, the green line is not present in these plots.

emission (Reynolds & Begelman 1997; Young et al. 1998; Fabian 2007). In this case, one would expect $f_{\rm Fe}$ to be inversely related to ionization, i.e., $f_{\rm Fe}$ should be a function of $\rho(R)/F_{\rm X}(R) \propto \rho(R)R^3$. More detailed calculations that solve for the vertical structure of the disk under hydrostatic equilibrium (e.g., Nayakshin et al. 2000; Nayakshin & Kazanas 2002) suggest that the line emission depends on a "gravity factor" $\sim(H/R^3)F_{\rm X}$. If that is the case, then for $F_{\rm X} \sim R^{-3}$, one expects the efficiency function $f_{\rm Fe}$ to be proportional to H.

In Figure 3, we compare the BR06 efficiency function $f_{\rm Fe(BR06)}$ (eq. [23]) to those suggested by our hydrostatic models, in the context of the constant-density and gravity theories mentioned above. Figure 3*a* shows $\rho(R)R^3$ as a function of radius. The line types/colors for the various models are the same as those defined in Figure 1. Superimposed on our density profiles is a thick short-dashed black line that represents $f_{\rm Fe(BR06)}$. For both $H/R = 0.01$ (*solid lines*) and 0.1 (*dotted lines*), and all values of α, we note that $\rho(R)R^3$ is an increasing function of radius, implying that $f_{\rm Fe}$ should also increase with increasing radius. There is no apparent reason why $f_{\rm Fe}$ should increase so steeply near the ISCO, or decrease at large radii, as suggested by $f_{\rm Fe(BR06)}$.

Figure 3*b* shows a similar plot for a rapidly spinning BH with $a_* = 0.95$. We notice the same trends as in Figure 3*a*. In this case, we also notice that (especially for $H/R = 0.1$), instead of becoming negligible at the ISCO, $\rho(R)R^3$ decreases gradually as one passes the ISCO and moves closer to the event horizon. Therefore, one does not expect $f_{\rm Fe}$ to drop abruptly to zero at the ISCO.

In Figures 3*c* and 3*d*, we consider the disk thickness in the inner region. In our models, the disk has a more or less constant thickness specified by H/R outside $\sim 100R_g$, and we vary this "outer thickness" by changing the value of f (eq. [19]). However, in the inner region, the disk gets thinner. Figure 3*c* shows H as a function of R for a nonspinning BH. The top panel of Figure 3*c* shows a disk with outer thickness of 0.01 and the bottom one shows a disk with outer thickness of 0.1 for the choices of α specified in § 3.1. In the thinner case, there is an abrupt drop in H, which would likely quench the iron emission from inside the ISCO. For the thicker case, however, the value of H decreases gradually and remains significant far inside the ISCO at $3R_g$. Thus, these models indicate that the region within the ISCO may contribute a significant fraction of the total iron line emission and, also, that it is difficult to justify the steeply falling form of $f_{\rm Fe(BR06)}$. As shown in Figure 3*d*, the results for a BH with $a_* = 0.95$ ($R_{\rm ISCO} = 1.973R_g$) are very similar. Again, for $H/R = 0.1$ the disk thickness H decreases gradually near and within the ISCO.

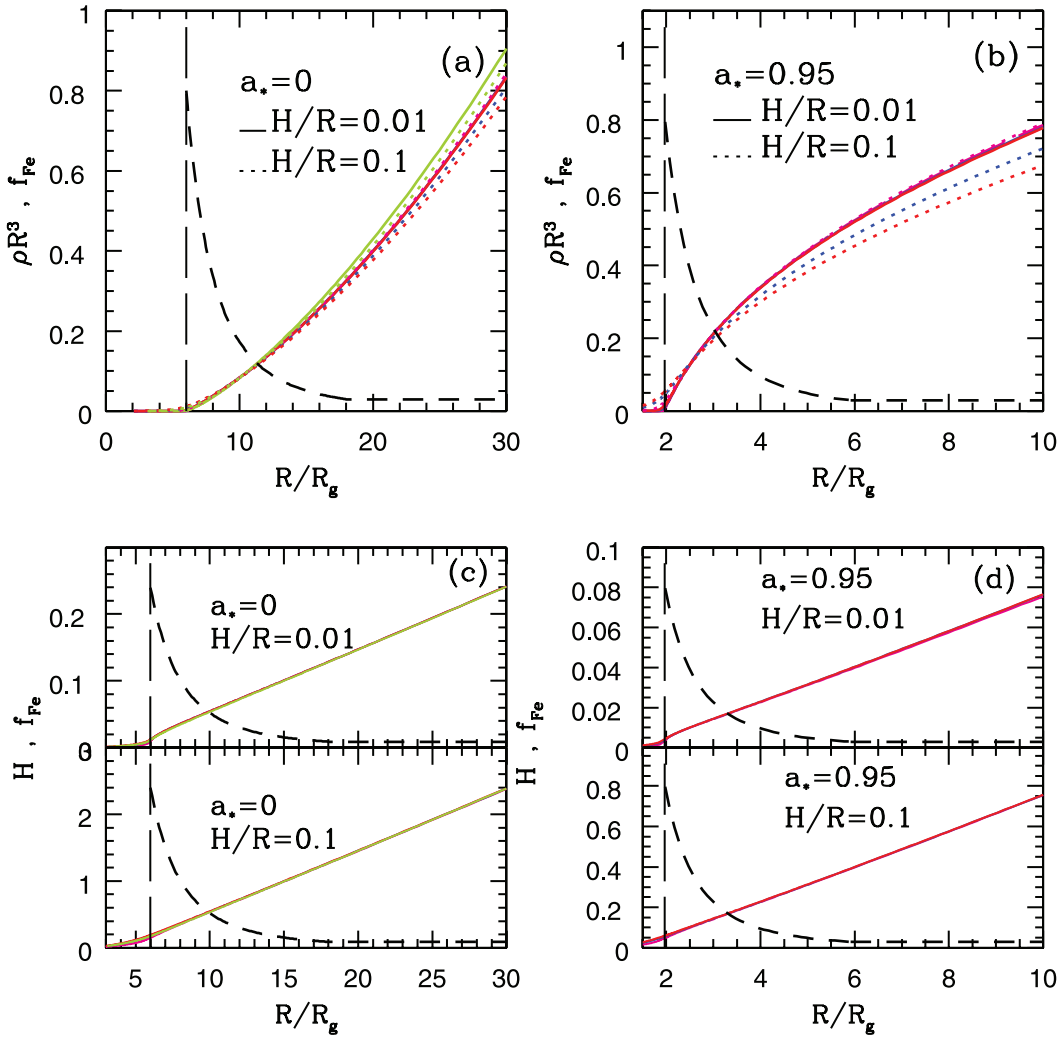

FIG. 3.—Profiles of $\rho(R)R^3$ (*a, b*) and disk thickness H (*c, d*) in the inner regions. For the line types/colors defining the various models and the location of the ISCO, see Figs. 1 and 2. Superimposed on our models in all of the panels is a thick black line that schematically represents the emissivity profile efficiency, $f_{\rm Fe}$, assumed in the iron line work in which the emissivity cuts off abruptly inside the ISCO and falls off as a steep power law outside the ISCO (eq. [23]). Panel (*a*) shows $\rho(R)R^3$ as a function of radius for a nonspinning BH. Panel (*b*) shows a similar plot for $a_* = 0.95$. Panels (*c*) and (*d*) show disk thickness H as a function of radius for $a_* = 0$ and 0.95, respectively, for disks with asymptotic values of $H/R = 0.01$ and 0.1. In panels (*a*) and (*b*), the normalizations used for $H/R = 0.01$ and 0.1 are different.

We hasten to add that this is a very simple model of an accretion disk, perhaps too simple to address "surface phenomena" such as fluorescent iron line emission. Modulo this important caveat it seems that, for reasonable values of the model parameters, the iron line emission does not necessarily end at the ISCO, nor does it vary with radius outside the ISCO with anything like the functional form assumed in current fits of iron line data (e.g., BR06).

3.3. *Viscous Stress Near the ISCO*

Figure 4 shows the vertically integrated stress $2H\alpha P$ for a nonspinning BH. As shown in Figure 4*a*, all the models corresponding to a very thin disk are in close agreement with the standard model, i.e., the stress nearly vanishes at the ISCO even though we do not require this of the model. For the thicker disk shown in Figure 4*b*, the stress near and inside the ISCO increases, the effect becoming more important for larger values of α. Interestingly, for $\alpha = 0.01$, the magnitude of the peak stress is actually smaller than that predicted by the standard disk model.

As shown in Figure 5, our models for a spinning black hole display essentially this same dependence of stress on H/R and α. In both Figures 4 and 5, the presence of a nonzero viscous stress inside the ISCO implies a contribution to the observed spectrum that is not accounted for in the standard disk model. In § 4 we investigate the magnitude of this effect.

We now consider the effect of α and disk thickness on the eigenvalue j (§ 2.2), which is the specific angular momentum delivered to the black hole by the infalling matter. In the standard disk model, j is the Keplerian specific angular momentum at the ISCO because (1) matter is assumed to orbit at the Keplerian velocity and (2) the stress is assumed to vanish inside the ISCO. Neither assumption is made in our hydrodynamic models, and it is therefore of interest to consider how much the calculated values of j differ from the standard value. Table 1 summarizes the values of j for our different models. We note that j decreases with increasing H/R and α. That is, as the disk gets thicker or as α increases, more angular momentum is removed before matter falls into the BH. However, the effects are quite small, and the deviations are less than 1% in all cases.

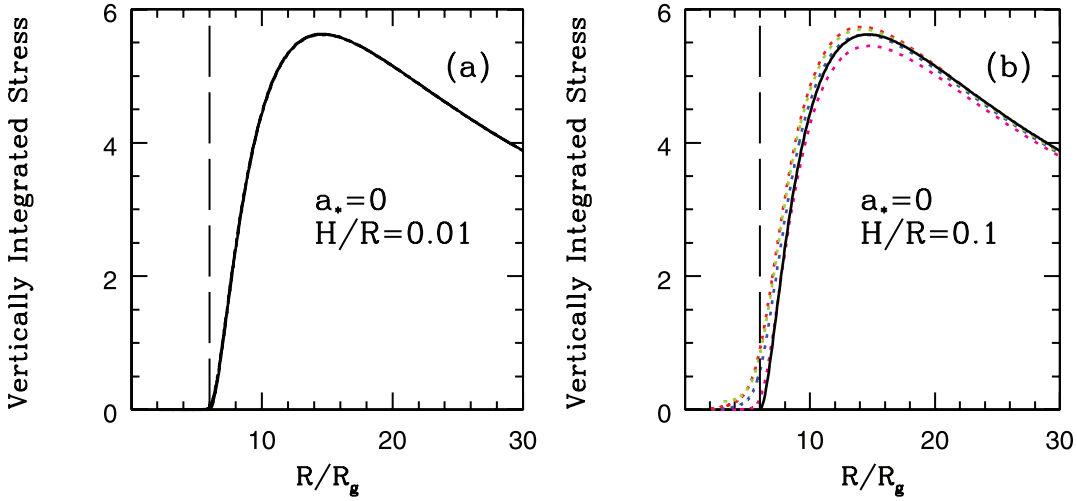

FIG. 4.—Vertically integrated stress $2H\alpha P(\times 10^4)$ for a nonspinning BH. In both panels the standard disk model is plotted as a thick solid line. For the line types/colors defining the various models and the location of the ISCO, see Fig. 1. (*a*) For $H/R = 0.01$, all four models are seen as indistinguishable from the standard model. (*b*) For the thicker disk, the models can be cleanly distinguished inside $R \sim 15R_g$. All numerical values correspond to $G = c = M = 1$, $\dot{M} = 1$.

3.4. *Dissipation inside the ISCO*

In § 3.3 we showed that the stress at the ISCO is small, but nonzero, and that it increases with disk thickness and α. We now consider the energy dissipation profiles of our model disks for different values of α and H/R. Figure 6 shows the quantity

$$R\frac{dL}{dR} = \frac{dL}{d\ln R} = \frac{-\dot{M}\alpha c_s^2 R^2}{v_R}\frac{d\Omega}{dR} = 4\pi R^2 D(R) \qquad (24)$$

as a function of R. Here L is the luminosity and $D(R)$ is the energy dissipated per unit time per unit surface area of the disk. Figures 6*a* and 6*b* show $R\,dL/dR$ versus R for $a_* = 0$, while Figures 6*c* and 6*d* show the results for $a_* = 0.95$. The solid black lines show the standard disk model with zero torque at the ISCO. For the thin disk with $H/R = 0.01$ and for all values of α, our models are indistinguishable from the standard model, which thus provides an excellent description of the flow in this case. However, for the thicker disk with $H/R = 0.1$, our numerical models deviate somewhat from the standard disk model. We note in particular that larger values of α are associated with more dissipation near the ISCO and larger deviations from the standard disk model.

In Table 1 we summarize the total luminosities of the different models for a given mass accretion rate $\dot{M}$. We note that none of the luminosities of our models deviates by more than 4% from that of the standard model.

4. DISK SPECTRA AND THE EFFECT ON BH SPIN ESTIMATION

In the standard disk model, the viscous dissipation is assumed to vanish at the ISCO. As a result, the emitted flux also vanishes at the ISCO, and no radiation is emitted from the region of the flow between the ISCO and the event horizon. For a given BH mass, the radius of the ISCO is a well-known and monotonically decreasing function of a_*, e.g., for $a_* = 0$ and 1, the ISCO is located at $6R_g$ and $1R_g$, respectively. As discussed in Zhang et al. (1997), S06, and M06, the radius $R_{\rm in}$ of the inner edge of the disk can be estimated from observations. For a BH of known mass, this radius can be expressed in units of R_g, and if the disk inner edge is located at the ISCO, then $R_{\rm in}/R_g$ determines the spin parameter a_*.

From the calculations presented in this paper, we see that for a very thin disk ($H/R = 0.01$) the viscous dissipation does indeed become negligible inside the ISCO and the dissipation profile $R\,dL/dR$ is identical to that predicted by the standard disk model.

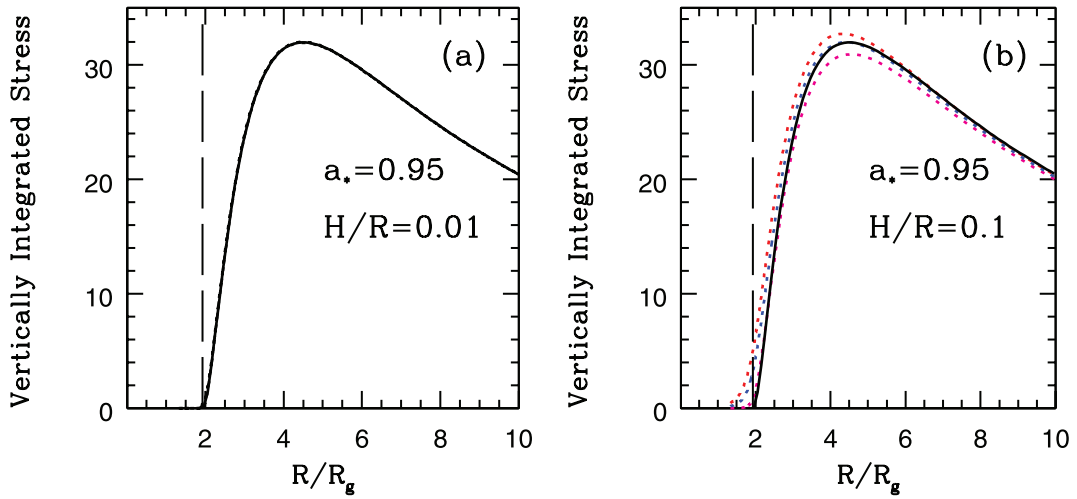

FIG. 5.—Same as Fig. 4, but for $a_* = 0.95$. As in Fig. 2, there is no variable-α model, and the ISCO is located at $R = 1.937R_g$.

TABLE 1
Luminosities and Angular Momentum Eigenvalues of the Numerical Disk Models

a_*	H/R	α	$L_{\rm tot}$ $(\dot{M}c^2)$	$L_{\rm tot\,(std)}$ $(\dot{M}c^2)$	j	$j_{\rm std}$
0.....	0.01	0.01	0.0624	0.0625	3.6744	3.6742
		0.1	0.0625		3.6735	
		0.2	0.0626		3.6727	
		Variable	0.0626		3.6730	
	0.1	0.01	0.0610		3.6839	
		0.1	0.0633		3.6609	
		0.2	0.0650		3.6456	
		Variable	0.0646		3.6518	
0.95.....	0.1	0.01	0.2091	0.2144	2.3372	2.3311
		0.1	0.2171		2.3237	
		0.2	0.2227		2.3146	

Note.—The subscript std refers to the standard thin disk model.

Thus, for such systems we expect our estimates of BH spin to be quite accurate. However, we do notice a difference for thicker disks with say $H/R \sim 0.1$. Using the standard disk model to fit the observed spectra of these systems will lead to an error in our estimate of the radius of the ISCO. We now try to quantify this error.

For each of our disk solutions, we have calculated the emitted spectrum assuming that the disk emits like a blackbody at each radius. The temperature profile $T(R)$ of the disk surface can be calculated from dL/dR using

$$(1-f)\frac{dL}{dR} = 4\pi\sigma R T^4(R), \tag{25}$$

where σ is the Stefan-Boltzmann constant. This can be used to calculate the observed spectrum of the disk by integrating over the entire disk,

$$F_\nu = \frac{2\pi\cos i}{D^2}\int_{R_{\rm inner}}^{R_{\rm out}} \frac{2h\nu^3 R\,dR}{c^2 e^{[h\nu/kT(R)]-1}}, \tag{26}$$

where h is the Planck constant, c the speed of light, k the Boltzmann constant, D the distance, i the angle of inclination, ν

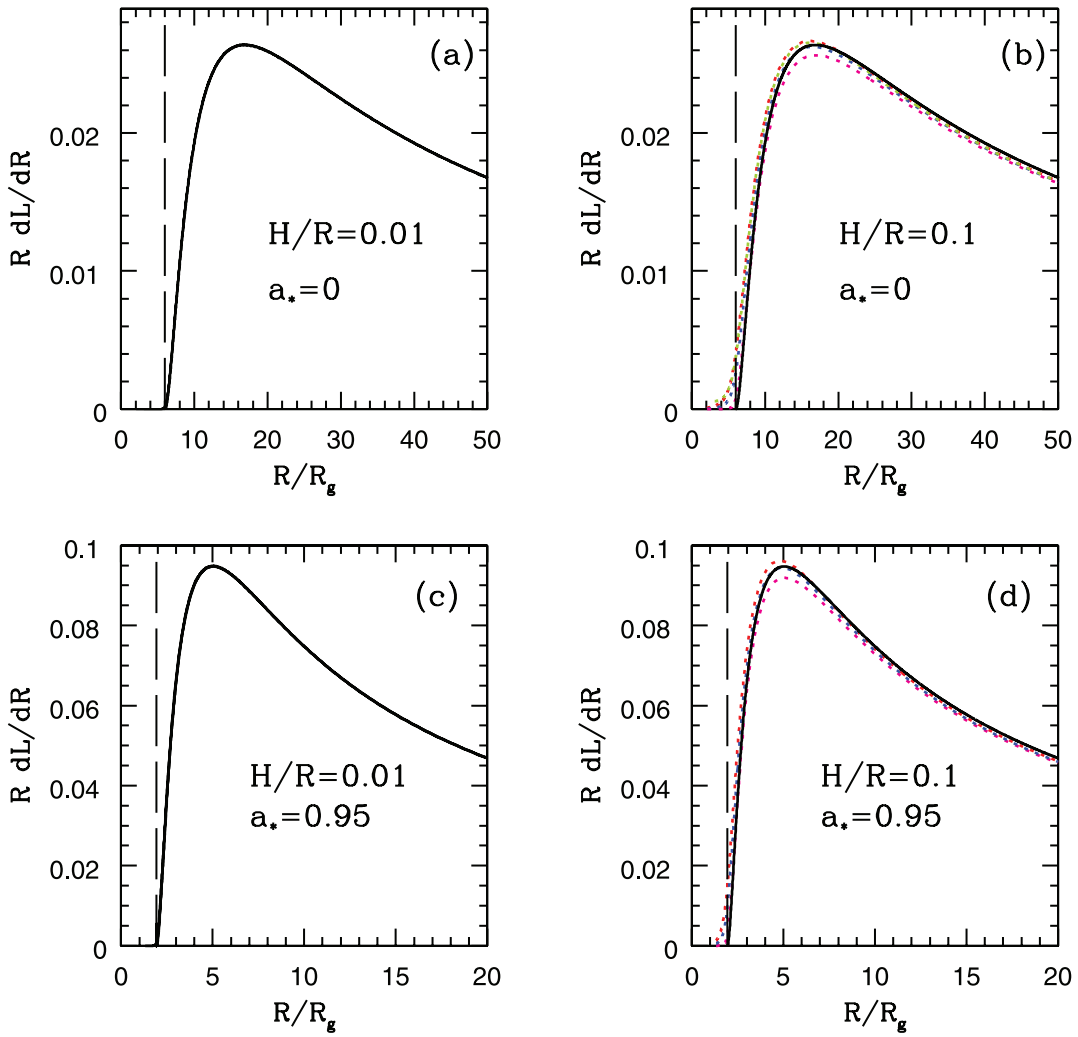

Fig. 6.—Rate of energy dissipation $R\,dL/dR$ as a function of radius R for models of a nonspinning BH (*a, b*) and a spinning BH (*c, d*). For the line types/colors defining the various models and the location of the ISCO, see Figs. 1 and 2. The models shown for the thinner disks coincide with the standard disk model, whereas the thicker disks deviate somewhat from the standard model.

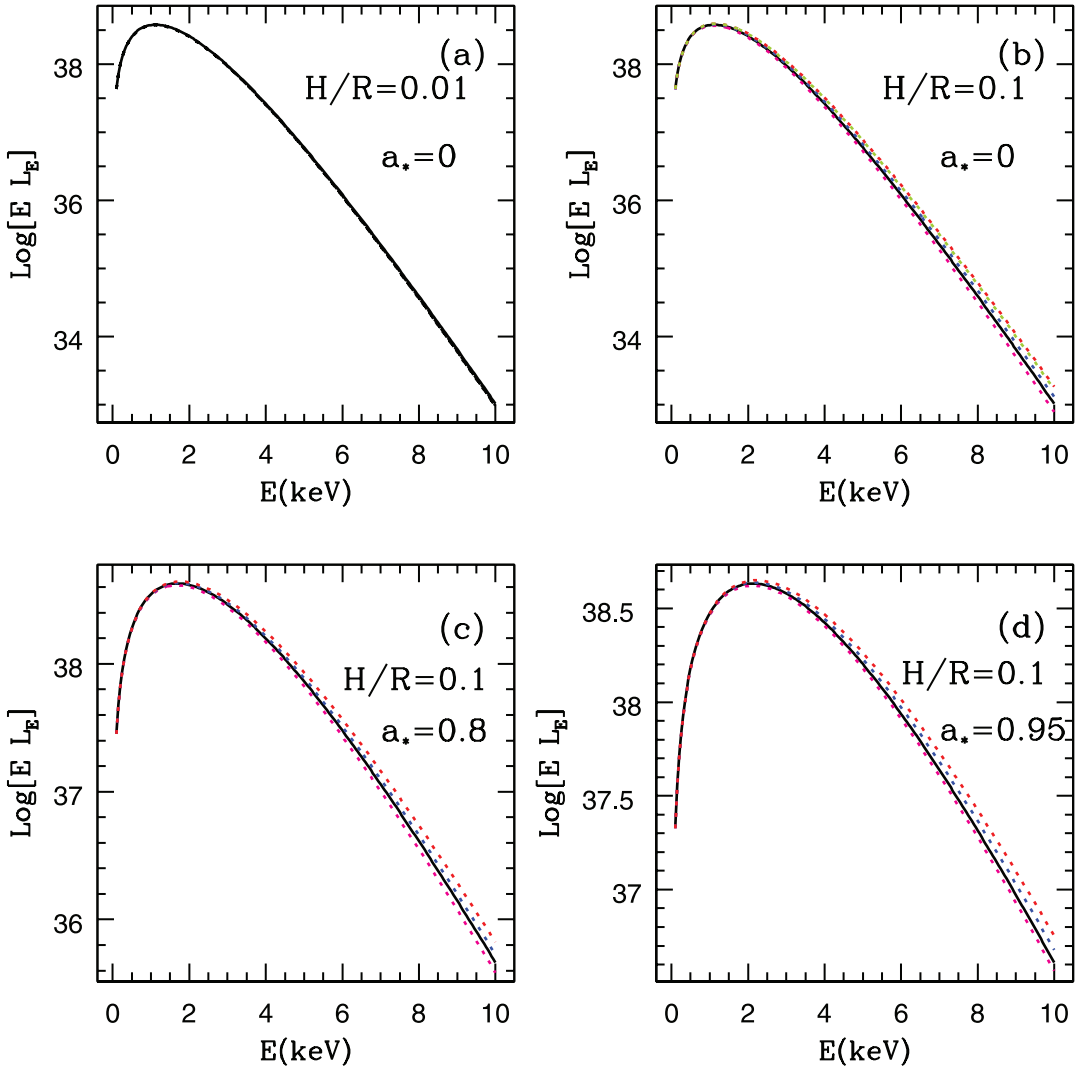

FIG. 7.—Spectra corresponding to the numerical disk models described in this paper for models of a nonspinning BH (*a, b*) and spinning BHs with thicker disks for $a_* = 0.8$ (*c*) and $a_* = 0.95$ (*d*). For the line types/colors defining the various models, see Figs. 1 and 2. Again, the different models are essentially indistinguishable in the case of the thin disk (*a*).

the frequency, and $R_{\rm inner}$ the radius of the inner boundary of the disk, near the event horizon.

Figure 7 shows our calculated spectra for a BH with mass $M = 10\ M_\odot$ and distance $D = 10$ kpc. In each panel the solid line shows the spectrum from a standard disk model with the appropriate pseudo-Newtonian potential. As before, we have considered three constant values of α, 0.01, 0.1, and 0.2, for both the spinning and nonspinning cases, and an additional variable-α model for the nonspinning case.

Figures 7*a* and 7*b* show the calculated spectra for the case of a nonspinning BH. For $H/R = 0.01$, we see that the calculated spectra for all four models of α overlap with the spectrum calculated via the standard disk model. Therefore, we can conclude that, for such very thin disks, the standard disk model is a very good approximation and that the choice of α cannot be a major source of error in estimating BH spin. The different lines are more distinct in the case of a thicker disk with $H/R = 0.1$ (magenta, blue, red, and green lines show the $\alpha = 0.01$, 0.1, 0.2, and variable-α models). The differences are especially noticeable at high photon energies, where larger values of α give higher fluxes. Figures 7*c* and 7*d* show $H/R = 0.1$ disk spectra for $a_* = 0.8$ and 0.95.

To estimate how the spectral distortions might affect BH spin determination, we produced spectral data files for our models using an *RXTE* response file and analyzed the data with XSPEC version 12.2.0. These "fake" data files were fitted with the XSPEC model Diskpn (Gierlinski et al. 1999), which uses the standard disk model with the PW80 potential and a zero-torque boundary condition at the ISCO. Diskpn has three fit parameters, $T_{\rm max}$, $R_{\rm in}/R_g$, and normalization $K = M^2 \cos i/D^2\beta$, where M is the mass, D the distance, i the angle of inclination, and β the color correction factor. We are interested in the case when the inner edge of the disk coincides with the ISCO. Thus, since Diskpn considers a nonspinning BH, we set $R_{\rm in} = 6R_g$. The constant K can then be rewritten as

$$K = \left(\frac{R_{\rm in}}{8.86\times10^6\ {\rm cm}}\right)^2 \left(\frac{D}{10\ {\rm kpc}}\right)^{-2} \frac{\cos i}{\beta}. \qquad (27)$$

In the above expression, 8.86×10^6 cm corresponds to $6R_g = R_{\rm ISCO}$ for a nonspinning black hole with $M = 10\ M_\odot$. From the value of K obtained from spectral fitting, one can calculate $R_{\rm in}$ for each model using equation (27). Using this value of $R_{\rm in}$, one can then calculate the BH spin for which the ISCO would be

TABLE 2
Errors in Spin Estimation of a Nonspinning BH

H/R	α	$R_{\rm in}/(8.86\times10^6$ cm)	Δa_*
0.01	0.01	1.011	−0.011
	0.1	1.008	−0.008
	0.2	1.006	−0.006
	Variable	1.007	−0.004
0.1	0.01	1.021	−0.019
	0.1	0.960	0.037
	0.2	0.920	0.074
	Variable	0.879	0.060

located at that radius. This is the spin that one infers from the fake spectral data, under the assumption that the standard disk model is correct. Since the model was calculated with full viscous hydrodynamics as described in previous sections, the spin value derived assuming the standard disk model will be different from the true BH spin ($a_* = 0$ in this case). The difference between the two values represents the error in the spin estimate, Δa_*, caused by our use of the simplified standard disk model.

The results of this analysis are summarized in Table 2. The results correspond to $M = 10\ M_\odot$, $D = 10$ kpc, $\cos i = 1$, and $\beta = 1$.

Figure 8*a* shows the results in more detail for $H/R = 0.01$, 0.02, 0.04, 0.06, 0.08, and 0.1. Figure 8*b* shows the results for the variable-α model as a function of disk thickness. We see that the error is larger for thicker disks and also for larger values of α. However, even for the thickest case we considered, $H/R = 0.1$, and the largest value of $\alpha = 0.2$, the BH spin is overestimated by less than 0.1. Thus, in the case of a nonspinning BH the error is quite modest when one considers, for example, that both the radius of the ISCO and the binding energy at the ISCO differ only slightly (by 6%) for a BH with $a_* = 0.1$.

Although a similar standard pseudo-Kerr XSPEC model is not available for fitting our spinning BH model spectra, it is still possible to estimate Δa_* by calculating the model luminosities. Gierlinski et al. (1999) showed that, for a nonspinning BH with the PW80 potential, one can write

$$L = \frac{1}{16}\dot{M}c^2 = 35.7\frac{\pi\sigma}{\beta^4}R_{\rm in}^2 T_{\rm max}^4, \tag{28}$$

where L is the luminosity, σ the Stefan-Boltzmann constant, β the color correction factor, $R_{\rm in}$ the radius of the inner edge of the disk, and $T_{\rm max}$ the peak temperature of the disk. Therefore, instead of calculating the multicolor blackbody spectrum of our models and fitting them with XSPEC, we could simply compare each hydrodynamic model with the corresponding standard disk model with the same $T_{\rm max}$. This gives the following estimate for the effective disk inner radius $R_{\rm in}$ of any given hydrodynamic model,

$$R_{\rm in}^2 = \frac{L_{\rm model}}{L_{\rm sd}}R_{\rm ISCO}^2, \tag{29}$$

where $L_{\rm model}$ is the luminosity of the model, $L_{\rm sd}$ is the luminosity of the standard disk with the same value of $T_{\rm max}$, and $R_{\rm ISCO}$ is the radius of the ISCO. The value of $R_{\rm in}$ obtained using equation (29) may then be used to calculate Δa_*, as before.

Figure 9*a* shows Δa_* values calculated using both the full spectral fitting method via equation (27) and the simpler luminosity-temperature method described by equation (29). We see that the results are very close, indicating that the second method is a good proxy for the more detailed spectral method.

For a spinning BH, equation (28) can be generalized to

$$L = \epsilon\dot{M}c^2 \sim c_0\frac{\pi\sigma}{\beta^4}R_{\rm in}^2 T_{\rm max}^4, \tag{30}$$

where ϵ is the spin-dependent efficiency of the BH and c_0 is a constant. Therefore, equation (29) can again be used to estimate the effective $R_{\rm in}$, and this can be used to obtain an estimate of the BH spin.

Figure 9*b* shows Δa_* for spinning BHs using this method. We show results for $a_* = 0.7$, 0.8, 0.9, and 0.95, and $H/R = 0.1$. For a given disk thickness and α, we see that the error in the spin estimate becomes smaller as the spin of the BH increases. For $a_* = 0.95$, the maximum error is only $\sim$0.01.

5. DISCUSSION

In this paper we studied the properties of a simple hydrodynamic model of an accretion disk using the α prescription for viscosity. We considered models with finite thicknesses H/R and different values of α. Our aim was to investigate how much the

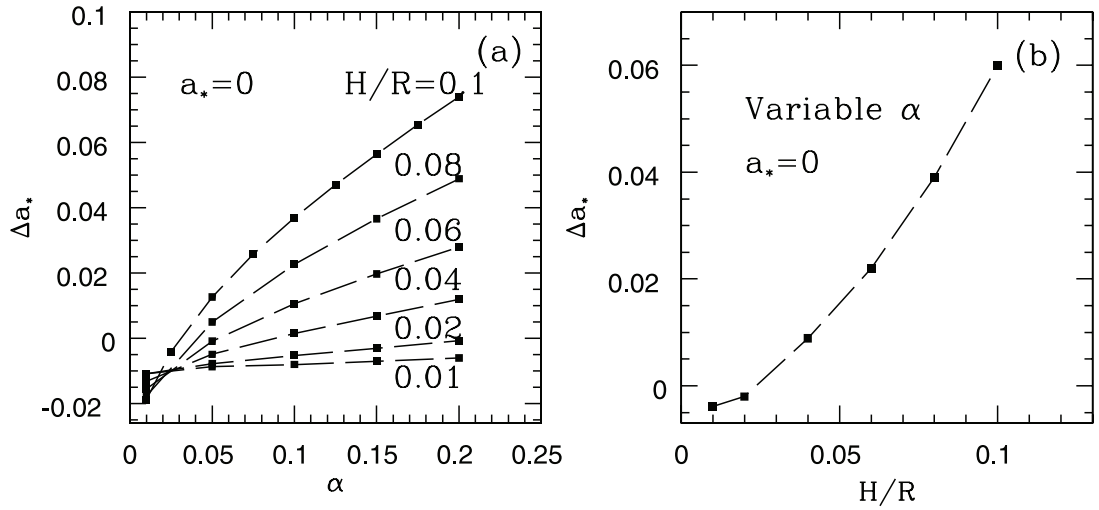

Fig. 8.—(*a*) Error in the spin estimate as a function of α for a BH with a true spin parameter of $a_* = 0$. The quantity Δa_* is equal to the value of a_* obtained from fitting the model spectrum minus the true a_*. The different lines correspond to different relative thicknesses H/R of the disk. (*b*) Error in the spin estimate for the variable-α profile as a function of disk thickness. In (*a*), note the variable offset from zero error that occurs near $\alpha = 0.01$, which is not visible in the previous figures for which the different α models nearly coincide with the standard disk model.

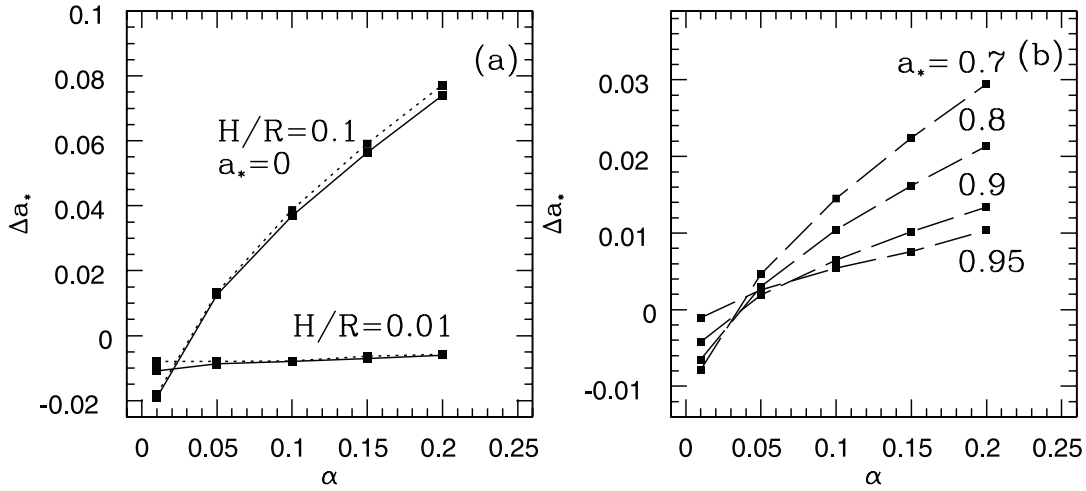

FIG. 9.—(*a*) Error in the spin estimate Δa_* for a nonspinning BH, calculated using spectral fitting and eq. (27) (*solid lines*) and from eq. (29) (*dotted lines*). The agreement is very good, showing that the simpler approach via eq. (29) is quite accurate. (*b*) Plots of Δa_* as a function of α for BHs with different values of a_*, calculated using eq. (29).

hydrodynamic models of thin disks deviate from the idealized "standard disk model" which assumes a vanishing torque at the innermost stable circular orbit (ISCO).

We find that the deviations of the viscous hydrodynamic models from the standard disk model increase with increasing H/R and increasing α. However, even for $H/R = 0.1$ and $\alpha = 0.2$, the largest values we tried for our thin disk calculations, the deviations remain modest. This is illustrated in Figures 4 and 5, which show how the stress profile deviates from that of the idealized standard disk model, and also in Figure 6, which compares the profiles of the viscous energy dissipation rate RdL/dR, Figure 7, which shows the multicolor blackbody spectra of the models, and Table 1, which gives some quantitative results. In all cases, we see that the detailed hydrodynamic models match the standard disk model quite closely.

We were motivated to do this study because we and others have used the standard disk model to fit the continuum spectra of BH X-ray binaries in the thermal state in order to estimate the spins of the BHs. How much error do we expect in the estimated spin values as a result of the fact that a real disk deviates from the standard disk model? At least for the simple hydrodynamic models we have considered in this paper, the answer is that the errors are quite modest.

Quantitative results are given in Table 2 and Figures 8 and 9. The error Δa_* in the derived estimate of BH spin is at most ~ 0.1 in the case of a nonspinning BH and is much less for rapidly spinning BHs. These errors are comparable to or smaller than the errors that arise from uncertainties in our estimates of mass, distance, and disk inclination (S06; M06).

While these results are very encouraging for our program to estimate BH spin through fitting the continuum spectra of BH accretion disks in the thermal state, we must note some caveats. First and foremost, we have considered a highly simplified toy hydrodynamic model with an α prescription for viscosity. Real disks doubtless have magnetic fields, and the stresses associated with these fields probably do not behave like microscopic viscosity. Indeed, it is precisely this argument that has been used by Krolik (1999), Gammie (1999), and HK02 to question the zero-torque boundary condition at the ISCO. On the other hand, Paczyński (2000) makes an equally persuasive argument (based on the angular momentum conservation equation) that, so long as the shear stress is smaller than the pressure, a thin disk will always satisfy the zero-torque condition.

In an attempt to include some of the effects of magnetic fields, we have considered a model in which we allowed α to vary with radius (see eq. [22]) in such a manner as to closely mimic the effective α obtained by HK02 from their MHD simulations. Even though in this model α increases rapidly with decreasing radius, especially inside the ISCO, we found that none of our results changed. Based on this finding we cautiously suggest that the inclusion of magnetic fields may not significantly alter our conclusions.

One question that needs to be addressed is why our results differ so much from those obtained by HK02. From MHD simulations of magnetized gas accreting in a PW80 potential, those authors concluded that the vertically integrated magnetic stress increases monotonically with decreasing radius all the way through and inside the ISCO. This is dramatically different from the behavior we find, as a comparison of HK02's Figure 10 with our Figure 4 shows. A likely explanation is that we have limited our study to *thin* disks ($H/R = 0.01$ and 0.1) in which we simulated strong cooling by choosing a small value for the advection parameter f (see the discussion below eq. [19]). HK02, by contrast, had no cooling in their MHD simulation, so their gas retained whatever energy was generated through shocks, making their disk thicker.

In order to verify that this difference is important, we calculated models with larger values of f using our viscous hydrodynamic code. It is hard to know what effective value of f is most appropriate to match the HK02 simulation. Nominally, theirs was a fully advection-dominated accretion flow, since they had no cooling at all; this means that their simulation corresponded to $f = 1$. However, we do not know how well their code conserved energy. Therefore, we calculated three models with $f = 1, 0.5$, and 0.25, all with the variable-α prescription (eq. [22]) which most closely matches their stress profile. Figure 10 shows the resulting stress profiles. We see that these advection-dominated models do exhibit a monotonically increasing stress inward, exactly as found by HK02 (their Fig. 10). The stress profiles are very different from those we find for cooling-dominated thin disks (our Figs. 4 and 5). Thus, we tentatively suggest that a large part of the difference between the results we find in this paper and those obtained by HK02 is related to the differing treatments of the energy equation of the gas, viz., cooling-dominated thin disk regime versus advection-dominated thick disk regime. In other words, we confirm the original insight of Abramowicz & Kato (1989), Paczyński (2000), and Afshordi & Paczyński (2003) on the strong relation between disk thickness and the stress at the ISCO. However, only

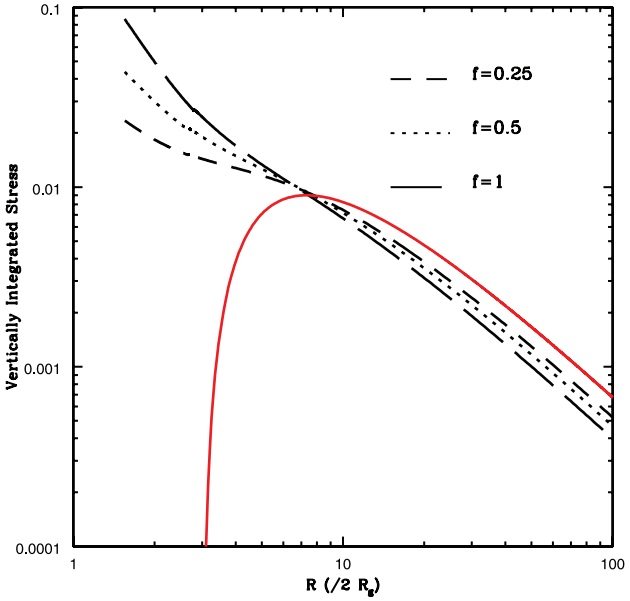

FIG. 10.—Vertically integrated stress profile as predicted by the standard disk model for a nonspinning BH (PW80 potential; *thick red solid line*). The other lines show the stress profiles of three hydrodynamic disk models with advection parameter values $f = 0.25$ (*short-dashed line*), 0.5 (*dotted line*), and 1 (*long-dashed line*). All three models use the variable-α prescription (eq. [22]), and their stress profiles have been scaled to match the standard model at $R = 15R_g$. A logarithmic scale has been used to facilitate comparison with the MHD simulation result shown in Fig. 10 of HK02.

a detailed MHD study of an accretion disk with significant cooling can tell for sure if this interpretation is correct, and to our knowledge nobody has carried out such a study.

Another limitation in our work is that we used a Newtonian model and we simplified the thermodynamics of the gas in the disk via the advection parameter f (see eq. [10]). However, doing the calculations in general relativity with full radiation thermodynamics will, we believe, introduce modifications only of order unity. The changes will be larger for a spinning BH, which we modeled with the Mukhopadhyay (2002) model, compared to a nonspinning hole (PW80 potential), but we think the error will still be only of order unity. Therefore, calculating these effects in more detail will not greatly alter our qualitative conclusion that the standard disk model is adequate so long as the disk is geometrically thin. Nevertheless, it would be useful to extend this work using a more complete set of disk equations, such as those employed in the study of slim disks (Abramowicz et al. 1988), and with the inclusion of general relativity (e.g., Abramowicz et al. 1997).

Note that we employed the two pseudo-Newtonian potentials mentioned above in the work reported here merely to obtain a ballpark estimate of the error associated with the zero-torque approximation. When we actually fit data to estimate the spin parameters of BHs (e.g., S06; M06), we use a detailed model (Li et al. 2005) which assumes the Kerr metric and includes all special relativistic and general relativistic effects.

In our work on BH spin (S06; M06), we limited ourselves to disks with luminosities less than 30% of Eddington, which corresponds to vertical thicknesses $H/R < 0.1$. The present study shows that this was a reasonable choice. For $H/R \leq 0.1$, the effects of gas physics and finite vertical thickness in our hydrodynamic models are not serious. Equally clearly, for thicker disks with H/R much greater than 0.1, the effects will be large; e.g., see Figure 10. Therefore, one should be cautious about applying the standard disk model to disks more luminous than 30% of Eddington. For this reason, we believe the results obtained by Middleton et al. (2006) for the spin of the microquasar GRS 1915+105 should be taken with caution.

Strong observational evidence that fitting the X-ray continuum is a promising way to estimate black hole spin comes from a long history of fitting the broadband spectra of black hole transients using the simple nonrelativistic multicolor disk model (Mitsuda et al. 1984; Makishima et al. 1986), which returns the temperature $T_{\rm in}$ at the inner disk radius $R_{\rm in}$. In their classic review, Tanaka & Lewin (1995) give examples of the steady decay (by factors of 10–100) of the thermal flux of transient sources during which $R_{\rm in}$ remains constant. They remark that the constancy of $R_{\rm in}$ suggests that it is related to the radius of the ISCO. More recently, this evidence for a constant inner radius in the thermal state has been presented for a number of sources via plots showing that the bolometric luminosity of the thermal component is approximately proportional to $T_{\rm in}^4$ (Kubota & Makishima 2001, 2004; Abe et al. 2005; McClintock et al. 2007). In short, these nonrelativistic analyses, which ignore spectral hardening (Davis et al. 2006), provide evidence for the presence of a stable radius, although they obviously cannot provide a secure value for the radius of the ISCO or even establish that the stable radius is the ISCO.

We now consider the iron line method of estimating spin. In this method, it is assumed that the line emission ceases abruptly at the ISCO, so an important question is whether or not the gas inside the ISCO will fluoresce (Reynolds & Begelman 1997). The possibility of line emission from inside the ISCO is usually discounted on the grounds that the density will fall suddenly inside the ISCO, thus causing a sudden increase in the ionization parameter (Fabian 2007 and references therein). Alternatively, and to the same effect, it is argued that emissivity is related to the "gravity parameter" (Nayakshin et al. 2000; Nayakshin & Kazanas 2002) and should depend on H. We see in Figure 3*a* that the density-dependent function $\rho(R)R^3$ does become negligible inside the ISCO for the nonspinning BH. However, that is not the case for a fast spinning BH with $a_* = 0.95$ (Fig. 3*b*) even for a small disk thickness of $H/R = 0.1$. In addition, the radial dependence of H shown in Figures 3*c* and 3*d* implies that there should be emission from the inner region unless the disk is very thin ($H/R = 0.01$).

An additional complication for iron line modeling is that the emissivity is assumed to vary as a broken power law, with the maximum emission occurring exactly at the ISCO (e.g., BR06). Looking at Figure 3, such an ad hoc model would be hard to justify if the emissivity has anything to do with gas density or disk thickness. In contrast, the continuum fitting model has the merit that it makes use of a physically motivated profile of disk emission $R\,dL/dR$ which can be calculated from first principles in the standard disk model and which continues to be valid even in the more general hydrodynamic models described in this paper (Figs. 6 and 7).

This paper has focused on only one aspect of BH spin estimation, viz., the validity of assumptions made in various methods of spin determination regarding the hydrodynamical properties of the accretion disk. Of course, a successful determination of spin needs more than a valid disk model. It also requires high-quality data and accurate determination of secondary system parameters. A discussion of these issues is beyond the scope of this paper, and the reader is referred to appropriate papers in the literature (e.g., M06; BR06).

The authors thank Niayesh Afshordi and Jonathan McKinney for discussions and useful suggestions. We dedicate this paper to Bohdan Paczyński for his amazing insights in accretion theory and in numerous other areas of astrophysics.

REFERENCES

Abe, Y., Fukazawa, Y., Kubota, A., Kasama, D., & Makishima, K. 2005, PASJ, 57, 629
Abramowicz, M. A., Czerny, B., Lasota, J. P., & Szuszkiewicz, E. 1988, ApJ, 332, 646
Abramowicz, M. A., & Kato, S. 1989, ApJ, 336, 304
Abramowicz, M. A., Lanza, A., & Percival, M. J. 1997, ApJ, 479, 179
Afshordi, N., & Paczyński, B. 2003, ApJ, 592, 354
Balbus, S. A., & Hawley, J. F. 1991, ApJ, 376, 214
Brenneman, L. W., & Reynolds, C. S. 2006, ApJ, 652, 1028 (BR06)
Chen, X., Abramowicz, M. A., & Lasota, J. P. 1997, ApJ, 476, 61
Chen, X., & Taam, R. E. 1993, ApJ, 412, 254
Davis, S. W., Blaes, O. M., Hubeny, I., & Tuner, N. J. 2005, ApJ, 621, 372
Davis, S. W., Done, C., & Blaes, O. M. 2006, ApJ, 647, 525
Fabian, A. C. 2007, in IAU Symp. 238, Black Holes: from Stars to Galaxies, ed. V. Karas & G. Matt (Cambridge: Cambridge Univ. Press), 129
Frank, J., King, A., & Raine, D. J. 2002, Accretion Power in Astrophysics (Cambridge: Cambridge Univ. Press)
Gammie, C. F. 1999, ApJ, 522, L57
Gierlinski, M., Zdziarski, A. A, Poutanen, J., Coppi, P. S., Ebisawa, K., & Johnson, W. N. 1999, MNRAS, 309, 496
Hawley, J. F., & Krolik, J. H. 2002, ApJ, 566, 164 (HK02)
Kato, S., Honma, F., & Matsumoto, R. 1988, MNRAS, 231, 37
Krolik, J. H. 1999, ApJ, 515, L73
Krolik, J. H., & Hawley, J. F. 2002, ApJ, 573, 754
Kubota, A., & Makishima, K. 2004, ApJ, 601, 428
Kubota, A., Makishima, K., & Ebisawa, K. 2001, ApJ, 560, L147
Li, L.-X., Zimmerman, E. R., Narayan, R., & McClintock, J. E. 2005, ApJS, 157, 335
Makishima, K., Maejima, Y., Mitsuda, K., Bradt, H. V., Remillard, R. A., Tuohy, I. R., Hoshi, R., & Nakagawa, M. 1986, ApJ, 308, 635
McClintock, J. E., Remillard, R. A., Rupen, M. P., Torres, M. A. P., Steeghs, D., Levine, A. M., & Orosz, J. A. 2007, ApJ, submitted (arXiv: 0705.1034)
McClintock, J. E., Shafee, R., Narayan, R., Remillard, R. A., Davis, S. W., & Li, L.-X. 2006, ApJ, 652, 518 (M06)
Middleton, M., Done, C., Gierliński, M., & Davis, S. W. 2006, MNRAS, 373, 1004
Mitsuda, K., et al. 1984, PASJ, 36, 741
Muchotrzeb, B., & Paczyński, B. 1982, Acta Astron., 32, 1
Mukhopadhyay, B. 2002, ApJ, 581, 427
Narayan, R., Kato, S., & Honma, F. 1997, ApJ, 476, 49
Narayan, R., & Popham, R. 1993, Nature, 362, 820
Narayan, R., & Yi, I. 1994, ApJ, 428, L13
Nayakshin, S., & Kazanas, D. 2002, ApJ, 567, 85
Nayakshin, S., Kazanas, D., & Kallman, T. 2000, ApJ, 537, 833
Paczyński, B. 2000, preprint (astro-ph/0004129)
Paczyński, B., & Bisnovatyi-Kogan, G. 1981, Acta Astron., 31, 283
Paczyński, B., & Wiita, P. J. 1980, A&A, 88, 23 (PW80)
Popham, R., & Narayan, R. 1991, ApJ, 370, 604
Quataert, E., & Narayan, R. 1999, ApJ, 516, 399
Remillard, R. A., & McClintock, J. E. 2006, ARA&A, 44, 49
Reynolds, C. S., & Begelman, M. C. 1997, ApJ, 488, 109
Ross, R. R., & Fabian, A. C. 1993, MNRAS, 261, 74
Ross, R. R., Fabian, A. C., & Young, A. J. 1999, MNRAS, 306, 461
Shafee, R., McClintock, J. E., Narayan, R., Davis, S. W., Li, L.-X., & Remillard, R. A. 2006, ApJ, 636, L113 (S06)
Shakura, N. I., & Sunyaev, R. A. 1973, A&A, 24, 337
Tanaka, Y., & Lewin, W. H. G. 1995, in X-Ray Binaries, ed. W. Lewin, J. van Paradijs, & E. van den Heuvel (Cambridge: Cambridge Univ. Press), 126
Young, A. J., Ross, R. R., & Fabian, A. C. 1998, MNRAS, 300, L11
Zhang, S. N., Cui, W., & Chen, W. 1997, ApJ, 482, L155
Życki, P. T., Krolik, J. H., Zdziarski, A. A., & Kallman, T. R. 1994, ApJ, 437, 597